Applied Catalysis B: Environmental 226 (2018) 451–462

Contents lists available at ScienceDirect

Applied Catalysis B: Environmental

journal homepage: www.elsevier.com/locate/apcatb

Greener synthesis of dimethyl carbonate using a novel tin-zirconia/graphene nanocomposite catalyst

Rim Saada[a], Omar AboElazayem[a,b], Suela Kellici[a], Tobias Heil[c], David Morgan[d], Giulio I. Lampronti[e], Basudeb Saha[a,*]

[a] Energy and Environment Research Centre, School of Engineering, London South Bank University, 103 Borough Road, London, SE1 0AA, UK
[b] Department of Chemical Engineering, British University in Egypt, El Sherouk City, Cairo 11837, Egypt
[c] Nanoinvestigation Centre at Liverpool, 1-3 Brownlow Street, Liverpool, L69 3GL, UK
[d] Cardiff Catalysis Institute, School of Chemistry, Cardiff University, Park Place, Cardiff, CF10 3AT, UK
[e] Department of Earth Sciences, University of Cambridge, Downing Street, Cambridge, CB2 3EQ, UK

ARTICLE INFO

Keywords:
Carbon dioxide utilization
Dimethyl carbonate
Propylene carbonate transesterification
Graphene nanocomposite
Heterogeneous catalyst
Continuous hydrothermal flow synthesis

ABSTRACT

A green, rapid and continuous hydrothermal flow synthesis (CHFS) route has been employed to synthesise highly efficient and active novel heterogeneous catalysts. Tin doped zirconia (Zr–Sn–O) and tin doped zirconia/graphene nanocomposite (Zr–Sn/GO) have been assessed as suitable heterogeneous catalysts for the synthesis of dimethyl carbonate (DMC). The catalysts have been extensively characterized using powder X-ray diffraction (XRD), transmission electron microscopy (TEM), Brunauer-Emmett-Teller (BET) surface area measurement and X-ray photoelectron spectroscopy (XPS) analysis. Extensive batch studies for the synthesis of DMC *via* the transesterification of propylene carbonate (PC) and methanol (MeOH) using Zr–Sn/GO catalyst in a solvent free process were also conducted. The effect of various reaction conditions such as reactant molar ratio, catalyst loading, reaction temperature and reaction time has been extensively evaluated. Response surface methodology based on Box-Behneken Design (BBD) was employed to derive optimum conditions for maximising PC conversion and DMC yield. The correlations and interactions between various variables such as MeOH:PC ratio, catalyst loading, reaction temperature, reaction time and stirring speed were extensively studied. A quadratic model by multiple regression analysis for the PC conversion and DMC yield was developed and verified by several methods BBD revealed that optimum conditions for high yield values of DMC are 12.33:1 MeOH:PC molar ratio, 446.7 K, 4.08 h and 300 rpm using 2.9% (w/w) Zr–Sn/GO nanocomposite. The maximum predicted responses at the optimum conditions are 85.1% and 81% for PC conversion and yield of DMC respectively. Experimental results at optimum model predicted reaction conditions agree very well with the model predicted response, where 82.4% PC conversion and 78.2% yield of DMC were obtained. Catalyst reusability and stability studies have been conducted at optimum reaction condition to investigate the long term stability of Zr–Sn/GO and it has been found that the catalyst could be reused more than six times (about 42 h) without losing its catalytic activity. These experimental and model predicted values showed an excellent agreement for tin doped zirconia/graphene nanocomposite as a heterogeneous catalyst for the synthesis of DMC from PC and MeOH.

1. Introduction

Dimethyl carbonate (DMC) is a promising environmentally benign compound that has gained considerable interests due to its versatile and excellent chemical properties. DMC's low toxicity and high biodegradability makes it a green reagent and a safer alternative to poisonous phosgene. Its high oxygen content (53%) makes it an excellent oxygenate additive to gasoline to improve its performance and reducing

Abbreviations: CHFS, continuous hydrothermal flow synthesis; Zr–Sn–O, tin doped zirconium oxide; Zr–Sn/GO, tin doped zirconia/graphene nanocomposite; DMC, dimethyl carbonate; XRD, X-ray powder diffraction; TEM, transmission electron microscopy; BET, Brunauer Emmett-Teller; XPS, X-ray photoelectron spectroscopy; PC, propylene carbonate; MeOH, methanol; BBD, Box-Behneken design; CO, carbon monoxide; O_2, oxygen; CO_2, carbon dioxide; RSM, Response Surface Methodology; IPA, isopropyl alcohol; $ZrO(NO_3)_2{\cdot}6H_2O$, zirconium(IV) oxynitrate; SnC_2O_4, tin (II) oxalate; HCl, hydrochloric acid (HCl); H_2SO_4, sulfuric acid; NGP, natural graphite powder; $NaNO_3$, sodium nitrate; H_2O_2, hydrogen peroxide; KOH, potassium hydroxide pellets; $KMnO_4$, potassium permanganate; GO, graphene oxide; HPLC, high performance liquid chromatography; GC, gas chromatography; FID, flame ionisation detector; ANOVA, analysis of variance; OFAT, ,one-factor at a time analysis

* Corresponding author.
E-mail address: b.saha@lsbu.ac.uk (B. Saha).

https://doi.org/10.1016/j.apcatb.2017.12.081
Received 3 August 2017; Received in revised form 20 December 2017; Accepted 31 December 2017
Available online 03 January 2018
0926-3373/

exhaust emissions [1]. DMC can be used as a good precursor material for the production of polycarbonates [2,3]. It can also be used as an intermediate in the synthesis of various pharmaceuticals and agricultural chemicals. Therefore, DMC is considered as an environmentally benign building block.

The conventional method for DMC synthesis involves the utilization of phosgene, a toxic feedstock. Thus, greener, safer and efficient processes for the synthesis of DMC are required. Recently, non-toxic synthetic routes have been explored; these include, oxidative carbonylation of carbon monoxide (CO), oxygen (O_2) and MeOH, direct synthesis from MeOH and CO_2 and the transesterification of cyclic carbonates and MeOH [4,5]. The oxidative carbonylation route suffers from the use of expensive raw materials and corrosive reagents as well as being potentially hazardous due to the explosive potential of CO. The direct production of DMC from MeOH and CO_2 offers an attractive and green synthetic route for DMC synthesis. However, this approach suffers from low DMC yields due to the equilibrium nature of the reaction and the un-reactivity of the stable CO_2 molecule. The synthesis of DMC *via* the transesterification of cyclic carbonates and MeOH has gained substantial interest recently, where cyclic carbonates can be synthesized from their corresponding epoxides and CO_2, thus making the synthesis of DMC *via* transesterification route more environmentally friendly and desirable in terms of green chemistry and sustainable development.

Much effort has been dedicated for the design of new greener catalytic processes for the synthesis of DMC. Several reports have been published describing the efficiency of various catalysts including alkali metal hydroxide [6], metal oxide [7], double metal cyanide [8], anion exchange resin [9], hydrotalcite [10,11], smectite [12], mesoporous carbon nitride [13], mesoporous ceria oxide [14], tungstate-based catalysts [15], ionic liquids [16] and gold nanoparticles [17].

Until now, ionic liquids have been reported to be the most efficient catalysts for transesterification of PC and MeOH [16,18,19]. However, the homogeneous nature of ionic liquids posed a number of drawbacks including high cost of separation of products/catalysts from the reaction mixture and challenges in terms of catalyst stability and reusability [20,21]. Therefore, the development of solvent-less heterogeneous catalytic process for the synthesis of DMC is highly desired and a key aspect for the design of greener chemical synthesis. Heterogeneous catalysts offer numerous advantages including the ease of catalyst separation from the reaction mixture, which is more economically viable due to the elimination of complex separation processes. Heterogeneous catalysts have higher stability, longer shelf life and easier and safer to handle, reuse and dispose compared to the homogenous counterpart [22]. However, advanced, low cost catalysts that perform efficiently are needed.

The (re)discovery of graphene [23,24], a single sheet of hexagonally arrayed sp^2-bonded carbon atoms, by Geim and Novoselov introduced a new era in materials science, the epoch of the 2D materials with applications in transformative technologies including catalysis [20,21,25]. Graphene success revealed that it is possible to obtain a stable, one-atom thick 2D material from layered van der Waals solids with fascinating unique physical, chemical and mechanical properties [24,26–28]. The exciting properties of graphene, such as very high surface area, chemical stability, excellent electrical and thermal conductivity, make graphene a very interesting material for a broad range of potential applications [29] including energy storage and generation (e.g. electrodes for lithium ion batteries, super capacitors, solar and fuel cells) [30–33], optical devices and high speed electronics [29,34,35], as well as CO_2 conversion technologies (e.g. catalysts and absorbers) [25] and biomedical field (sensors, antibacterial) [36,37]. However, the 2D material alone does not possess the properties that are required in a range of technological applications. Owning to the flexible yet robust 2D membranes, it is possible to design and construct novel 2D based functional materials with superior or different properties from parent 2D material. This can be efficiently achieved *via* bottom–up approaches and structural functionalization incorporating 2D materials with nanoparticles or forming nanocomposites [27,30,38,39]. However, making sheets of high quality 2D and strongly coupled homogeneous nanocomposites in an economical and environmentally benign way is still challenging. The current methods for making 2D nanomaterial composites (e.g. homogenization by mixing of inorganic nanoparticles and grinding) can be difficult in order to obtain very well dispersed nanoparticles in good electrical contact with the 2D nanosheets. Thus, the preparation of high quality graphene related materials with desirable functional properties through green synthetic routes is a highly desirable step, since the presence of defects will influence the properties and consequently its applications.

Building from our recent work [20,21,37], the approach for making 2D based nanocomposites uses a clean, rapid technology. It utilises a green, rapid and Continuous Hydrothermal Flow Synthesis (CHFS) route [40–43] for the synthesis of 2D-inorganic nanocomposites with superior properties to those currently available. This will afford advanced functional materials with minimal structural and electronic defects. CHFS reactors offer significant advantages over traditional synthetic methods such as independent control over reaction parameters (e.g. temperature and pressure) and hence particle properties. The CHFS process involves mixing a continuous stream of superheated or supercritical water with a continuous flow of aqueous metal salt(s) to give rapid precipitation and controlled growth of nanoparticles at a defined mixing region [44–46]. A key feature of this process is the way of which the properties of water (such as density, diffusivity and dielectric constant) change dramatically around the critical temperature and pressure (647 K, 22.1 MPa) leading to its use as an exotic, highly controllable reaction solvent/medium. The composition and particle properties can thus be modulated by independently controlling the process parameters such as the ratios and concentrations of any metal salt feeds, flow rates of feeds, pressure, and temperature of mixing and the presence of pH/redox modifiers or surfactants [47]. The 2D plate like structure of the materials of interest offers an attractive substrate for deposition of inorganic nanoparticles for highly dispersed composites with novel properties. Thus, by feeding water dispersions of 2D material into a CHFS process before nucleation it will be possible to fully integrate these two materials into true nanocomposites.

In recent years, Response Surface Methodology (RSM) has been employed to evaluate the relationship between multiple process variables in order to optimise a specified response (i.e. output variable) [48,49]. Applying RSM at experimental stage reduces the number of experimental trials and hence the overall cost of the experiments. RSM is a collection of mathematical and mathematical techniques based on multivariate statistics, which includes experimental design, statistical model and process optimization [50]. RSM has a track record in helping researchers in modelling and optimization of the experimental design for various applications in food industry, catalysis and chemical reaction optimisation [51]. It helps to conclude the most important factors and their direct and interacted effects on the response. A further advantage of using RSM is that it does not require theoretical knowledge or human experience and still could accurately mimic the trends using the design experimental results satisfactorily.

In this study, an innovative approach has been employed for synthesizing advanced heterogeneous catalysts such as mixed metal oxides and graphene-inorganic nanocomposite catalyst *via* utilization of a continuous hydrothermal flow synthesis (CHFS) reactor. The catalytic performance of the synthesized catalysts has been extensively studied for a greener and sustainable route for the synthesis of DMC. RSM using BBD has been conducted for process modelling and optimization, with an aim to better understand the relationships between five operating variables (MeOH:PC molar ratio, catalyst loading (w/w), reaction temperature, reaction time and stirring speed) and their impact on PC conversion and yield of DMC. Furthermore, regression analysis has been applied to establish the validated model used to derive the optimum operating conditions for DMC synthesis.

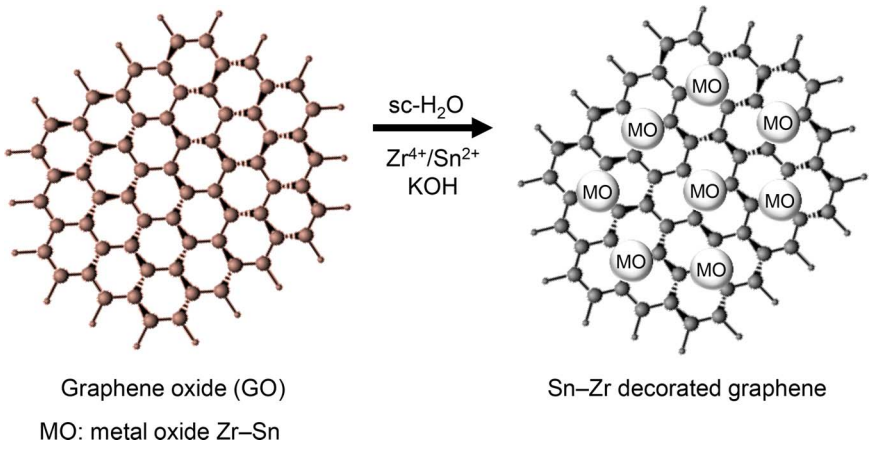

Fig. 1. A schematic representation of the synthesized Zr–Sn/graphene nanocomposite catalyst. Schematic representation of the synthesized Zr–Sn/graphene nanocomposite catalyst.

2. Experimental

2.1. Materials

Methanol (MeOH), propylene carbonate (PC), *iso*-propyl alcohol (IPA), dimethyl carbonate (DMC), zirconium(IV) oxynitrate hydrate ($ZrO(NO_3)_2{\cdot}6H_2O$, 99.99%) and tin (II) oxalate (SnC_2O_4, 98%) were purchased from Sigma-Aldrich Co. Ltd (UK). Other chemicals were purchased from Fisher Scientific, UK, including hydrochloric acid (HCl, 37%), sulphuric acid (H_2SO_4), natural graphite powder (NPG), sodium nitrate ($NaNO_3$, 98 +%), hydrogen peroxide (H_2O_2, > 30%), potassium hydroxide pellets (KOH, 86 +%) and potassium permanganate ($KMnO_4$, 99%). In all cases 10 MΩ deionised water was used. All chemicals were used without any further purification.

2.2. Catalyst preparation

Graphene oxide (GO) was synthesized using Hummer's method [20,21,37]. The as-prepared GO was then used as a precursor for the synthesis of tin doped–zirconium oxide/graphene nanocomposites (see Fig. 1) [Zr–Sn oxide/graphene, where nominal atomic ratio of Zr:Sn used was (9:1)] *via* CHFS, design of which has been reported elsewhere. The CHFS system utilises three high performance liquid chromatography (HPLC) pumps for the delivery of aqueous solution of precursors as shown in Fig. 2. Pump 1 (Gilson 307 fitted with 25 mL pump head) was used for pumping deionized water through a custom made electrically powered pre-heater (723 K) at a flow rate of 20 mL min^{-1}. Pumps 2 and 3 (Varian Pro Star 210 fitted with 5 mL pump head) delivered pre-sonicated aqueous GO solution premixed with corresponding tin and zirconium salts at the desired ratio and KOH, respectively, where both pumps were operated at a flow rate of 5 mL min^{-1}. Typically, tin doped–zirconium oxide/graphene nanocomposites were synthesized *via* the following synthetic approach: pre-mixed aqueous solutions of $ZrO(NO_3)_2{\cdot}6H_2O$ and SnC_2O_4 (with a total metal ion concentration of 0.2 M and molar ratios of 9:1) and a pre-sonicated (60 min) aqueous solution of GO (4 μg mL^{-1}) were pumped to meet a flow of KOH (1 M) at a T-junction (see Fig. 2). The ratio used were Zr^{4+}/Sn^{2+} = 1 and GO = 2. This composition was then brought into contact with superheated water (723 K, 24.1 MPa) inside a counter-current reactor, whereupon the formation of tin–zirconia oxide/graphene nanocomposite occurred in a continuous manner. The aqueous suspension was cooled through the cooler (pipe-in-pipe design) and the slurries were collected from the exit of the back pressure regulator (utilised to maintain a reactor pressure of 24.8 MPa throughout the experiment). After collection, the particles were centrifuged (4500 rpm) and washed twice with deionized water. The wet solids were then freeze–dried and subjected to further analysis and experimentation. For comparative purposes, pure Zr–Sn metal oxide was also synthesized following the same synthetic approach, but in the absence of graphene.

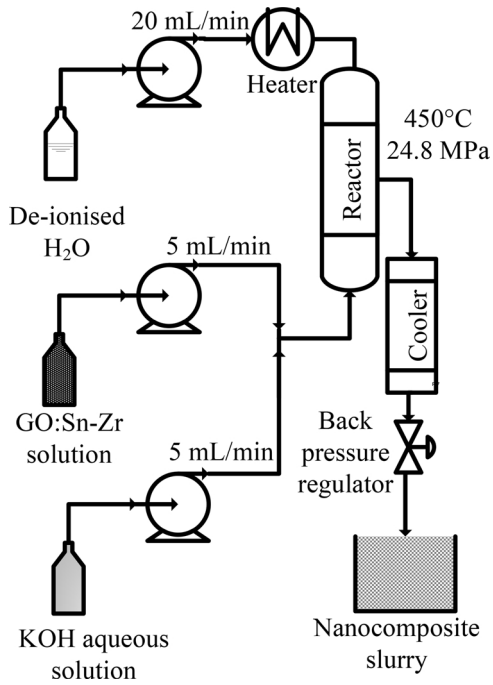

Fig. 2. Schematic of a CHFS reactor set-up used for the synthesis of Zr–Sn/graphene nanocomposite catalyst.

2.3. Catalyst characterisation equipment

Micromeritics Gemini VII analyzer (nitrogen adsorption and desorption method) was used to measure the BET surface area of the as prepared samples. The powders were degassed at 423 K in N_2 (purge gas supplied by BOC, UK) for 12 h prior to BET analysis. The particle size and morphology of as-prepared samples were investigated using a JEOL 2100FCs with a Schottky Field Emission Gun transmission electron microscope (200 kV accelerating Brunauer–Emmett–Teller (BET) surface area measurements of all samples were conducted on a voltage). Samples were collected on carbon-coated copper grids (Holey Carbon Film, 300 mesh Cu, Agar Scientific, Essex, UK) after being briefly dispersed ultrasonically in water. Particle size analysis was performed using ImageJ particle size analysis software. X-ray powder diffraction data were collected on a low background silicon sample holder in Bragg-Brentano geometry on a D8 Bruker diffractometer equipped with primary Gobbel mirrors for parallel Cu Ka X-rays and a Vantec position sensitive linear detector. Collection conditions were: 5 − 110° in 2θ,

0.04 step size, 450 s/step, divergence slits 0.6 mm. XPS measurements were performed using a Kratos Axis ultra DLD photoelectron spectrometer utilizing monochromatic Alka source operating at 144 W. Samples were mounted using conductive carbon tape. Survey and narrow scans were performed at constant pass energies of 160 and 40 eV, respectively. The base pressure of the system is *ca.* 1×10^{-9} Torr, rising to ca. 4×10^{-9} Torr under analysis of these samples.

2.4. Transesterification of propylene carbonate with MeOH

Transesterification reactions of PC with MeOH were carried out in a 25 mL autoclave reactor (model 4590, Parr Instrument Company, USA) equipped with a stirring system, a thermocouple (type J), a heating mantle and a controller (model 4848). In a typical experiment, different molar ratios of PC and MeOH along with the required amount of the heterogeneous catalyst were charged into the reactor vessel. The reactor was continuously stirred and heated to the required temperature for the desired reaction time. After the completion of the reaction, the reactor was cooled down to room temperature using an ice bath and the reaction mixture was filtered. The liquid products were analysed using a gas chromatography (Shimadzu GC–2014) equipped with a flame ionisation detector (FID) with a capillary column using *iso*-propyl alcohol as an internal standard. The effect of various reaction parameters were studied for the optimization of reaction conditions. The long term stability of the catalyst was assessed by carrying out catalyst reusability studies at the optimum conditions.

2.5. Method of analysis for transesterification reactions

The sample collected from the reaction mixture of propylene carbonate and methanol was analysed using a Shimadzu gas chromatography (GC–2014). A ramp method was used in order to separate all the compounds present in the sample mixture. The initial temperature of the oven was set at 323 K and the sample was injected by an auto sampler for analysis. The column temperature was then held at 323 K for 5 min after the sample had been injected. Afterwards, a temperature ramp was applied that increased at a rate of 50 K min^{-1} to a temperature of 523 K *n*-Pentane was used as a solvent to wash the injection needle after the sample injection. The subsequent sample runs were started when the column temperature was cooled back to 323 K. The components mass fractions were directly calculated from the chromatograms *via* internal standard method using IPA as an internal standard.

2.6. One-factor-at-a-time analysis (OFAT)

PC and MeOH transesterification reactions were carried out as described in section 2.4. OFAT analysis was developed to conclude the effective range of the factors in order to start statistical analysis within these ranges. The influence of five single factors (MeOH:PC molar ratio, catalyst loading, reaction temperature, reaction time and stirring rate) were evaluated for effective synthesis of DMC. The OFAT analysis investigated various MeOH: PC molar ratio (2:1, 4:1, 6:1, 8:1, 10:1, 12:1, 14:1), catalyst loading (%)(w/w) (1, 1.5, 2, 2.5, 3, 3.5), reaction temperature (K) (403, 413, 423, 433, 443, 453, 463), reaction time (h) (2, 4, 6, 8, 10) and stirring speed (rpm) (300, 400, 500).

2.7. Experimental design

Based on the OFAT method, the effective ranges of the independent factors were observed. The experimental runs were carried out according to five independent variables at 3 levels (3^5) factorial design, namely, MeOH:PC molar ratio, catalyst loading, reaction temperature, reaction time and stirring speed, which were labelled as X_1, X_2, X_3, X_4 and X_5 respectively. Codes were given for the levels of each variable (i.e., −1, 0, 1). The variables and their levels are presented in Table 1. Box-Behneken Design (BBD) is a method of response surface methodology (RSM) employed to examine the relationship between the factors and their direct and combined effect on responses [52]. Three levels-five variables BBD model was implemented for this study. The total number of experiments (N) is given by Eq. (1)

Table 1
Independent variables and their levels used in the response surface design.

Variables	Code	Levels		
		−1	0	+1
MeOH:PC molar ratio	X_1	6	10	14
Catalyst loading (%)(w/w)	X_2	1.5	2.5	3.5
Reaction temperature (K)	X_3	403	433	463
Reaction time (h)	X_4	2	4	6
Stirring speed (rpm)	X_5	300	400	500

$$N = k^2 + k + C_p \quad (1)$$

Where, k is the number of independent factors and C_p is the replicate number of the centre point. PC conversion and DMC yield were chosen as the responses for this study. The experiments were performed in a randomized order to minimize the influence of unexplained variability in the responses that caused by extraneous factor [53]. Table 2 shows the 46 experiments at various conditions and their corresponding responses which were used to develop the model.

2.8. Statistical analysis

A quadratic equation for the model is shown using Eq. (2):

$$Y = b_o + \sum_{i=1}^{3} b_i x_i + \sum_{i=1}^{3} b_{ii} x_i^2 + \sum_{i \neq j=1}^{3} b_{ij} x_i x_j \quad (2)$$

where Y is the dependent response, b_o is the model coefficient constant, b_i, b_{ii},b_{ij} are coefficients for intercept of linear, quadratic, interactive terms respectively, while X_i, X_j are independent variables (i ≠ j) [51]. The model was confirmed with the correlation coefficient (R^2), adjusted coefficient of determination (R^2_{adj}) and the predicted coefficient of determination (R^2_{pred}). Analysis of variance (ANOVA) was used to investigate the statistical significance of the regression coefficient by conducting the Fisher's F-test at 95% confidence level. The coefficient of determination (R^2) is defined as the regression of sum of squares proportion to the total sum or squares which illustrates the adequacy of a model. R^2 ranges from 0 to 1 and as the value of R^2 approaches 1, it indicates that the model is more accurate. The high adjusted and predicted coefficients of determination also illustrate whether the model adequately fits the data or not [54]. Design Expert 9.0.5 software (Stat-Ease Inc., Minneapolis, MN, USA) was used for the design of experiment, regression and graphical analysis. Statistical significance of the results have been presented by $p < 0.05$ and mean ± SE. The fit quality of the polynomial equation has been proved by R^2.

3. Results and discussion

3.1. Catalyst characterization

Herein, we have fostered an innovative CHFS approach in producing high quality 2D graphene nanocomposites *via* utilization of continuous hydrothermal flow of superheated water in alkaline medium in a single rapid synthetic route. Zr–Sn–O/GO nanocomposites were made from a 0.2 M (total concentration) of pre-mixed aqueous solution of tin oxalate and zinc nitrate (to produce Sn^{4+}: Zr^{4+} at 10:90 atomic ratio) and GO (made *via* conventional Hummers method) under alkaline conditions (KOH, 1 M). For comparative purposes, pure Zr–Sn oxide catalyst was also synthesized.

The particle size and morphology of as-prepared samples were

Table 2
Experimental results of the response surface methodology.

Run	A	B	C	D	E	PC conversion[a] (%)	PC conversion[b] (%)	DMC yield[a] (%)	DMC yield[b] (%)
1	14:1	2.5	433	4	300	73	70.3	70	67.7
2	14	1.5	433	4	400	49	47.6	48	46.7
3	10	2.5	433	2	300	35.5	38	33.7	35.6
4	10	2.5	433	4	400	76.2	76.2	72.2	72.2
5	10	2.5	463	4	500	69.5	67.2	67.3	64.8
6	10	1.5	433	6	400	52	50.1	49.3	47.8
7	10	2.5	433	2	500	35.5	37.9	33.6	36.1
8	10	1.5	463	4	400	44.9	44.4	42.8	42.4
9	6	2.5	433	2	400	14.2	12.6	13.7	12.2
10	10	3.5	403	4	400	14.9	16.5	13.8	14.9
11	6	1.5	433	4	400	25	26.5	23.8	24.8
12	10	2.5	463	2	400	25.6	22.2	24.2	21
13	10	1.5	403	4	400	9.1	8.1	8.6	7.3
14	10	2.5	463	6	400	74	76.3	70.8	72.8
15	10	2.5	403	4	300	21.9	24.7	20.6	23.2
16	10	1.5	433	2	400	20.9	22.9	19.5	21.5
17	10	2.5	433	4	400	76.2	76.2	72.2	72.2
18	10	3.5	433	6	400	74	72.2	70	68.3
19	6	2.5	463	4	400	29	28	26.5	25.9
20	6	2.5	433	4	300	40.9	41.3	38.3	38.9
21	6	3.5	433	4	400	34.1	34.2	32	31.9
22	10	2.5	403	2	400	3.1	2.2	2.2	1.6
23	10	3.5	463	4	400	63.2	65.4	59.9	61.9
24	10	2.5	403	4	500	22	22.8	20.7	21.2
25	10	1.5	433	4	500	52.9	53.7	50.3	51.3
26	14	2.5	433	6	400	72	75.3	71.1	73.8
27	6	2.5	433	6	400	35.1	36.7	33	34
28	10	3.5	433	2	400	28.2	30.2	26.3	28
29	10	2.5	433	4	400	76.2	76.2	72.2	72.1
30	14	2.5	433	2	400	30	30.1	28.8	29
31	10	2.5	463	4	300	65.9	65.5	62.1	61.7
32	14	3.5	433	4	400	72	69.2	69	66.6
33	6	2.5	433	4	500	40.1	42.2	38.4	40
34	10	3.5	433	4	300	69.1	68.5	64.8	64.2
35	10	2.5	403	6	400	12.5	14.2	11.7	13.2
36	10	2.5	433	6	300	75.2	72.6	71.2	68.8
37	10	1.5	433	4	300	52.9	53.5	50.3	50.7
38	10	2.5	433	4	400	76.2	76.2	72.2	72.2
39	14	2.5	403	4	400	12.1	13.4	11.7	13.1
40	10	2.5	433	4	400	76.2	76.2	72.2	72.2
41	10	3.5	433	4	500	68.5	68.1	64.9	64.8
42	14	2.5	463	4	400	68.3	71.5	67.1	70.1
43	14	2.5	433	4	500	70.3	69.3	69.2	67.8
44	6	2.5	403	4	400	3.9	3	3	2
45	10	2.5	433	6	500	75.2	72.6	71.2	69.5
46	10	2.5	433	4	400	76.2	76.2	72.1	72.1

A: MeOH:PC molar ratio.
B: Catalyst loading [%][w/w].
C: Reaction temperature [K].
D: Reaction time [h].
E: Stirring speed [rpm].
[a] Experimentally obtained.
[b] Predicted by model.

investigated by transmission electron microscopy (TEM) and the images are shown in Fig. 3. TEM images for pure Zr–Sn oxide (Fig. 3a) and the corresponding Zr–Sn oxide/GO nanocomposite (Fig. 3b) revealed uniform particles exhibiting a mean particle size of 4.80 ± 1.49 nm and 5.18 ± 0.91 nm, respectively. The TEM image for the graphene oxide (Fig. 3c) revealed a sheet/plate like morphology. The nanocatalyst exhibited moderately high BET surface areas of 148.39 $m^2 g^{-1}$, 83.32 $m^2 g^{-1}$ and 139.38 $m^2 g^{-1}$ for pure metal oxide, Zr–Sn/graphene and graphene oxide, respectively.

The crystallinity of the synthesized nanocomposite catalysts synthesized *via* CHFS was assessed by X-ray powder diffraction (XRD) and is shown in Fig. 4. The XRD pattern for both samples gave peaks corresponding to the zirconium oxide crystal structure.

To investigate the changes in the concentration of tin and zirconium in the lattice, their oxidation states and the chemical states of graphene oxide for all prepared catalysts, X-ray photoelectron spectroscopy (XPS) analysis was employed and the spectra of which are shown in Fig. 5. The XPS elemental analysis for all the samples showed peaks corresponding to tin, zirconium, oxygen and carbon. As previously reported, the CHFS approach is effective in dehydrating/reducing GO. Indeed, the deconvoluted C (1s) XPS spectra of Zr–Sn oxide/graphene nanocomposite showed considerable reduction in peak intensities of the oxygen-containing functional groups (carboxyl, epoxide and hydroxyl), which are associated with GO (starting material). Furthermore, the XPS analysis for Sn3d spectra revealed spin–orbit doublet peaks centred at *ca.* 487 eV ($3d_{5/2}$) and ca. 495 eV ($3d_{3/2}$) indicating the presence of Sn^{4+}, which was confirmed by analysis of the Auger peaks and the corresponding Auger parameter.

XPS spectrum of the Zr 3d core level showed a strong spin–orbit doublet, with the $3d_{5/2}$ peak at 182.3 eV and assigned to Zr^{4+}, which is in agreement with reported literature values and characteristic of Zr^{4+} ions in their full oxidation state.

3.2. Model development

Response surface methodology (RSM) is a set of statistical and mathematical techniques used for modelling and predicting the direct factors and their interaction that affects the response in order to develop the optimum conditions [55]. The influence of five variables, including, MeOH:PC molar ratio, catalyst loading, reaction temperature, reaction time and stirring speed on the responses (PC conversion and DMC yield) were evaluated using BBD method. Table 2 shows the experimental and predicted responses at various process conditions. A quadratic polynomial model was applied to build a mathematical model in order to combine the relationship between the responses and the independent factors. This was also used to determine the optimum reaction conditions for a maximum PC conversion and DMC yield. The developed quadratic model for the PC conversion and DMC yield are given in Eqs. (3) and (4) respectively.

$$Y_1 = -5933.96 - 5.71X_1 + 13.24X_2 + 27.19\,X_3 - 34.89\,X_4 + 0.037\,X_5 + 0.87X_1X_2 + 0.06X_1X_3 + 0.65X_1X_4 - 0.001X_1X_5 + 0.1X_2X_3 + 1.84X_2X_4 - 0.001X_2X_5 + 0.16X_3X_4 + 0.0002X_3X_5 + 1.3^{-17}X_4X_5 - 1.15X_1^2 - 13.36X_2^2 - 0.03X_3^2 - 4.75X_4^2 - 0.0001X_5^2 \quad (3)$$

$$Y_2 = -5580.42 - 8.82X_1 + 12.51\,X_2 + 25.71\,X_3 - 34.22\,X_4 - 0.043\,X_5 + 0.8\,X_1X_2 + 0.06X_1X_3 + 0.71X_1X_4 - 0.0005X_1X_5 + 0.09X_2X_3 + 1.74X_2X_4 + 0.0001X_2X_5 + 0.15X_3X_4 + 0.0004X_3X_5 + 0.0001X_4X_5 - 1.05X_1^2 - 12.75X_2^2 - 0.03X_3^2 - 4.5X_4^2 - 0.0001X_5^2 \quad (4)$$

Where, X_1, MeOH:PC molar ratio; X_2, catalyst loading (w/w)(%); X_3, reaction temperature (K); X_4, reaction time (h); X_5, stirring rate (rpm); Y_1, PC conversion (%) and Y_2 yield of DMC (%).

3.3. Statistical analysis

Statistical analysis was performed on DMC yield since it is the most important response. The regression model for DMC yield (Eq. (2)) was tested by ANOVA as shown in Table 3. The coefficient R^2 is used to define the fitness of the regression model. Adequate precision is defined to measure the signal to noise ratio where its value should be greater than 4 to ensure negligible noise [53]. The statistical analysis indicated that the developed model is highly significant due to high *F*-value (246.3) and very low *p*-value (< 0.0001). R^2 value was obtained as 0.995 and adequate precision of 42.2 which is extremely larger than the minimum required value of 4. The R^2_{pred} of 0.9798 is in reasonable agreement with the R^2_{Adj} 0.9909 since the difference is less than 0.02. The value of R^2_{adj} (0.995) shows a difference of 0.5% between the experimentally obtained and model predicted yield of DMC.

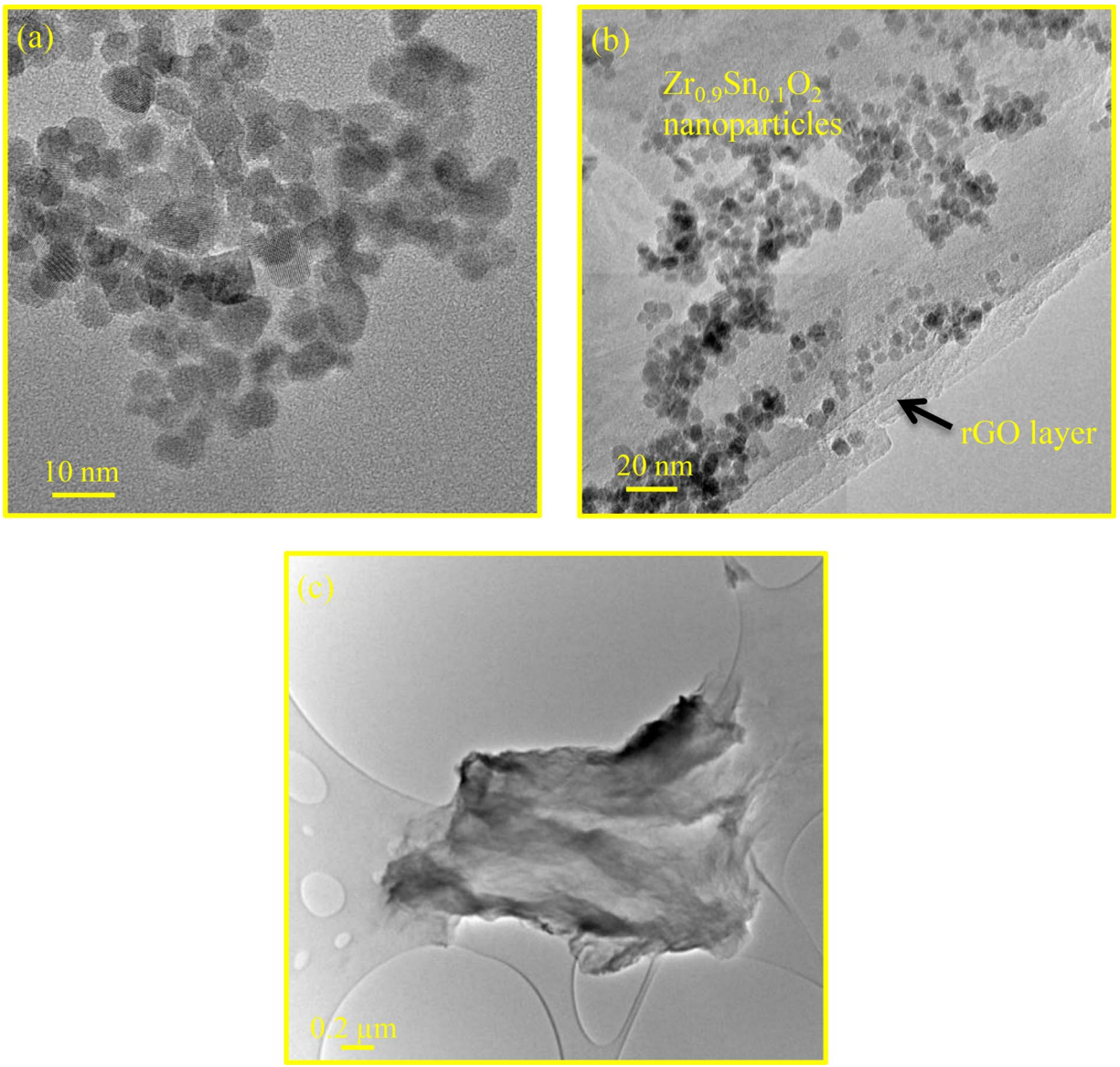

Fig. 3. Transmission Electron Microscopy (TEM) images of (a) pure metal of tin doped zirconium oxide (Zr–Sn–O) (b) tin doped zirconia/graphene nanocomposite (Zr–Sn/GO) (c) graphene oxide (GO) sample.

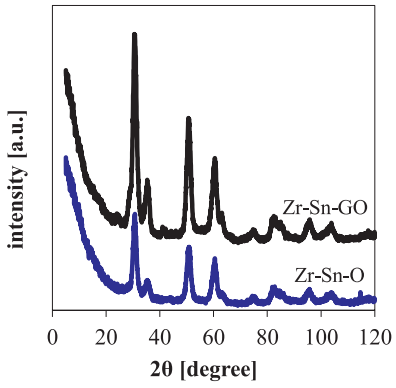

Fig. 4. X-ray powder diffraction (XRD) patterns of tin doped zirconium oxide (Zr–Sn–O) (b) tin doped zirconia/graphene nanocomposite (Zr–Sn/GO).

Based on the validity analysis of the factors it can be concluded that the independent variables (X_1, X_2, X_3, X_4), the interaction variables (X_1X_2, X_1X_3, X_1X_4, X_2X_3, X_2X_4, X_3X_4), the quadratic variables (X_1^2, X_2^2, X_3^2, X_4^2, X_5^2) are significant factors for the synthesis on DMC. Stirring rate (X_5) and its interactions with other variable are insignificant but its quadratic effect (X_5^2) is significant. The insignificance of stirring speed (X_5) and its interactions indicate very low effect on the yield of DMC.

3.4. Model validation

The results obtained from the ANOVA test indicate that the developed model is suitable to describe the correlations and interactions of the different variables and the yield of DMC. Fig. 6 shows the experimental *vs* predicted yield of DMC and illustrates that the model equation is in a good agreement with the experimental data indicating the suitability and accuracy of the model. BBD model was used to predict the effect of various design parameters on DMC synthesis from PC and MeOH. The results are presented in Figs. 8–12. The results confirmed that BBD predicted the experimental results accurately at various reaction conditions.

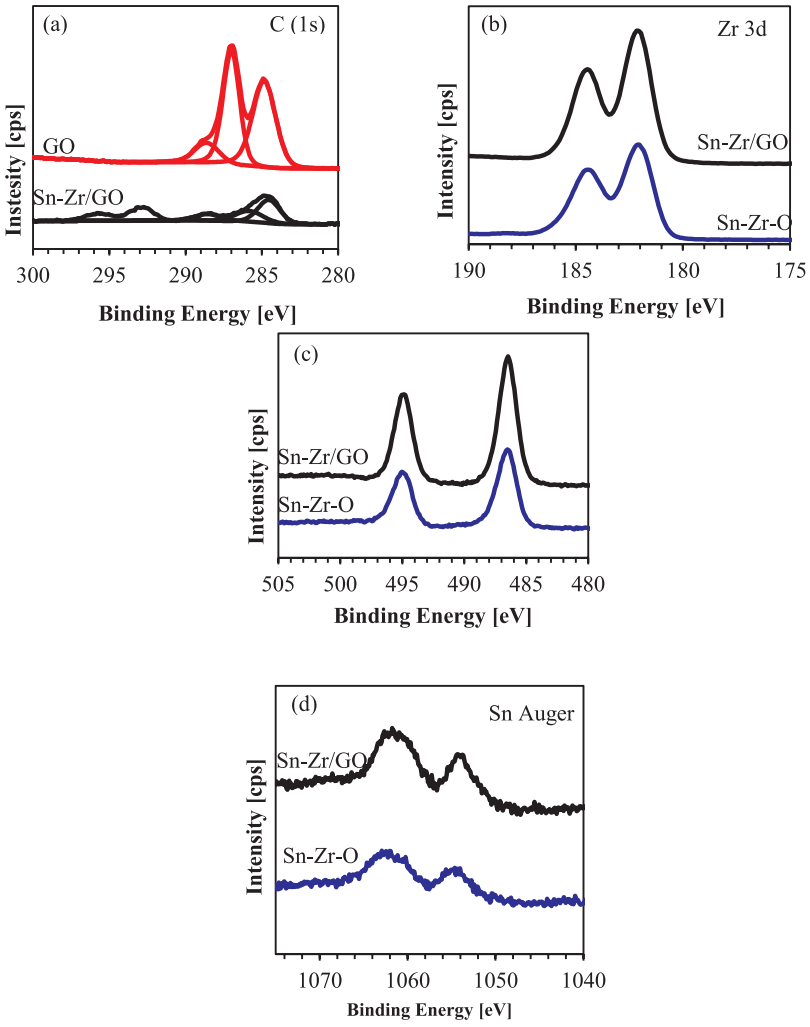

Fig. 5. X-ray photoelectron spectroscopy (XPS) spectra showing (a) deconvoluted C(1s), (b) Zr (3d) region, (c) Sn(3d) region and (d) Sn Auger parameter region.

3.5. Batch experimental results

The reaction scheme for the synthesis of DMC *via* transesterification of propylene carbonate with methanol in the presence of a suitable catalyst is shown in pathway 1 of Fig. 7. Propylene glycol (PG) is the main co-product which is produced in equimolar quantity to DMC and, therefore, it has been exempted from the discussion. Dimethyl ether (DME) and propylene oxide (PO) are the expected side products from the reaction of PC and MeOH [16,56–58]. DME was below the detection limit of the GC–FID used for the analysis of experimental samples and therefore its specific yield was not calculated. This observation is similar to the work published before [1,59]. PO was not detected as a side product in this study.

Transesterification reactions of PC to MeOH were carried out at different reaction conditions in the presence of Zr–Sn/graphene nanocomposite as catalysts. OFAT analysis was carried out to study the effect of reactant molar ratio, catalyst loading, reaction temperature and time on the yield of DMC. Reusability studies were conducted to evaluate the long term stability of Zr–Sn/GO nanocomposite catalyst for the synthesis of DMC.

3.5.1. Effect of different catalysts

The performance of various different heterogeneous catalysts was assessed for the effective synthesis of DMC from the reaction of PC and MeOH as shown in Fig. 8, where all experiments were conducted using 10:1 MeOH:PC molar ratio, 10% (w/w) catalyst loading, 433 K, 4 h at 300 rpm. Pure metal of tin doped zirconium oxide (Zr–Sn–O) and tin doped zirconia/graphene nanocomposite (Zr–Sn/GO) were synthesized using CHFS method. Zr–Sn/GO samples were heat treated at 773 K and 973 K to enhance their catalytic activity and labelled as HT500 and HT700 respectively. When the pure metal oxide was used to catalyse the transesterification reaction, PC conversion and yield of DMC were 45.4% and 38.9%, respectively. Incorporating graphene oxide in the formation on inorganic nanocomposite resulted in high catalytic performance of Zr–Sn/GO, with a PC conversion of 76.2% and DMC yield of 72.1%. The difference in the catalytic performance between Zr–Sn–O and Zr–Sn/GO can be attributed to the phase composition and of the catalyst alongside with the defects on the graphene sheet such as holes, acid/basic groups and presence of residual which can provide additional active catalytic sites [25]. HT500 and HT700 were tested at the same reaction condition as Zr–Sn/GO and showed insignificant increase in both PC conversion and yield of DMC (± 3%). From energy efficiency view point, the increase in DMC yield is insufficient to carry out the heat treatment. Therefore, on the basis of this study, Zr–Sn/GO was found to be the best catalyst for the synthesis of DMC and was used for further studies.

3.5.2. Effect of reactant molar ratio

In order to evaluate the dependence of the catalytic performance on the reaction reactant molar ratio, a set of catalytic reactions was conducted in the presence of Zr–Sn/GO nanocomposite catalyst using various molar ratio of methanol to propylene carbonate (MeOH:PC). The experiments were carried out using 2.5% (w/w) catalyst loading at 433 K for 4 h. The first experiment was carried out (as part of the OFAT)

Table 3
ANOVA for response surface quadratic model analysis of variance.

Source	Sum of squares	Degrees of freedom	Mean square	*F* value	*p*-value
Model	25219.9	20	1261.0	246.3	< 0.0001 hs
A	3195.4	1	3195.4	624.2	< 0.0001 hs
B	729.9	1	729.9	142.6	< 0.0001 hs
C	6741.8	1	6741.8	1316.9	< 0.0001 hs
D	4429.9	1	4429.9	865.3	< 0.0001 hs
E	1.3	1	1.3	0.3	0.621 ns
AB	41.2	1	41.2	8.0	0.008 s
AC	255.2	1	255.2	49.8	< 0.0001 hs
AD	131.9	1	131.9	25.8	< 0.0001 hs
AE	0.2	1	0.2	0.0	0.843 ns
BC	35.4	1	35.4	6.9	0.0144 s
BD	48.6	1	48.6	9.5	0.0049 s
BE	0.0	1	0.0	0.0	0.988 ns
CD	344.5	1	344.5	67.3	< 0.0001 hs
CE	6.4	1	6.4	1.3	0.272 ns
DE	0.0	1	0.0	0.0	0.982 ns
A^2	2489.5	1	2489.5	486.3	< 0.0001 hs
B^2	1418.9	1	1418.9	277.2	< 0.0001 hs
C^2	6734.7	1	6734.7	1315.5	< 0.0001 hs
D^2	2828.6	1	2828.6	552.5	< 0.0001 hs
E^2	23.8	1	23.8	4.6	0.04 s

A: MeOH:PC molar ratio.
B: Catalyst loading [%][w/w].
C: Reaction temperature [K].
D: Reaction time [h].
E: Stirring speed [rpm].
s: significant.
ns: not significant.
hs: highly significant.

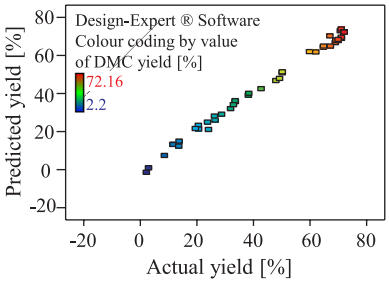

Fig. 6. Model predicted DMC yield *vs* experimentally obtained DMC yield.

at low MeOH:PC molar ratio (2:1) where a PC conversion of ~17.2% and ~13.2% yield of DMC were observed. OFAT analysis showed that the reactant molar ratio almost exhibits a linear relationship with catalytic performance of the transesterification reaction as ~76.2% conversion of PC and ~72.2% yield of DMC were obtained for higher MeOH:PC molar ratio (10:1). The significant increase in the yield of DMC with an increase in the MeOH:PC molar ratio can be attributed to the formation of DMC–MeOH azeotrope due to the presence of excess MeOH which shifts the equilibrium towards the product side and enhances the synthesis of DMC [56]. Fig. 9 shows the effect of increasing MeOH:PC ratio within the range of 6:1 to 14:1 on the PC conversion and yield of DMC. It is evident that when the reactant molar ratio (MeOH:PC) increased to 12:1 and 14:1 (Fig. 9), there was insignificant change to the yield of DMC when compared to MeOH:PC molar ratio of 10:1. On the basis of this study, it can be concluded that the optimum MeOH:PC ratio is 10:1 for the catalysed system. This is within the range reported in the literature for the transesterification of PC with MeOH by other investigators [8,11].

3.5.3. Effect of catalyst loading

In this study, catalyst loading is defined as the percentage ratio of the mass of the catalyst to the mass of the limiting reactant (PC). The synthesis of DMC *via* the transesterification of PC and MeOH was studied using different amounts of Zr–Sn/GO nanocomposite catalyst at 433 K for 4 h. The results are presented in Fig. 10. It is noted that an increase in the catalyst loading increases the PC conversion and yield of DMC. For reactions carried out using 1.0% (w/w) catalyst loading, PC conversion and DMC yield were ~43.8% and ~41.6% respectively. Further increase in the conversion of PC (~76.2%) and yield of DMC (~72.2) were achieved at 2.5% (w/w) catalyst loading. When the catalyst loading was further increased to 3% (w/w), PC conversion of ~76.5% and DMC yield of ~72.3% were achieved. In view of the experimental error of ± 3%, it seems that the number of active sites required for PC and MeOH to react and produce DMC was sufficient at 2.5% (w/w) catalyst loading. Hence it was not necessary to increase the catalyst loading beyond 2.5% (w/w). Based on this study 2.5% (w/w) of Zr–Sn–O/GO nanocomposite was chosen as the optimum catalyst loading and was used in all subsequent experiments.

3.5.4. Effect of reaction temperature

A series of transesterification reaction of PC and MeOH were conducted within a temperature range of 403 K and 463 K to thoroughly investigate the influence of reaction temperature on the synthesis of DMC. The experiments were carried out using MeOH:PC ratio is 10:1 in the presence of 2.5% (w/w) Zr–Sn/GO nanocomposite catalyst for 4 h. Fig. 11 shows the effect of reaction temperature on the conversion of PC and the yield of DMC. It can be seen from Fig. 11 that the reaction temperature has a pronounced effect on the efficiency of DMC synthesis.

As the reaction temperature increased from 413 K to 433 K, there was a significant increase in the PC conversion and yield of DMC. At a reaction temperature of 433 K, the conversion of PC and yield of DMC were ~76.2% and ~72.2%, respectively. At reaction temperatures higher than 433 K, a linear decrease in both PC conversion and yield of DMC was observed. This decrease is possibly due to the equilibrium nature of the transesterification reaction where higher reaction temperatures can shift the equilibrium to the reactant side and results in a reduction to the yield of DMC [60]. Therefore, it can be concluded that 433 K is the optimum reaction temperature and all further OFAT experiments for the synthesis of DMC were performed at a reaction temperature of 433 K. The optimum reaction temperature is within the range of published literature [7,8,60].

3.5.5. Effect of reaction time

A set of transesterification reactions were carried out using the best performed catalyst (Zr–Sn/GO) for different time duration (2 h–6 h) to evaluate the influence of the reaction time on the DMC synthesis. The results are presented in Fig. 12. The reaction proceeds at low reaction time (2 h) and results in a PC conversion of ~30.1% and ~28.8% yield of DMC. An increase in the reaction time significantly increases the conversion of PC to ~76.2% and the yield of DMC to ~72.2%. A similar PC conversion and DMC yield were obtained when the reaction was carried out for 6 h. As the reaction time increased beyond 6 h, PC conversion and DMC yield begin to decline gradually indicating that equilibrium is reached at 4–6 h. This study indicates that 4 h reaction time is sufficient to reach equilibrium and to achieve the maximum DMC yield and therefore, 4 h was considered as the optimum reaction time for the transesterification of PC.

3.5.6. Effect of external mass transfer in heterogeneous catalytic processes

The effect of mass transfer resistance on the transesterification reaction of PC and MeOH using Zr–Sn/GO nanocomposite catalyst to produce DMC was investigated at 433 K reaction temperature for 4 h. The reaction of PC and MeOH was conducted at different stirring speed of 300–500 rpm in an autoclave reactor as shown in Fig. 13. It was observed that there was no significant change in the conversion of PC and yield of DMC when the stirring speed increased from 300 to 500 rpm. These results are in good agreement with the BBD predicted

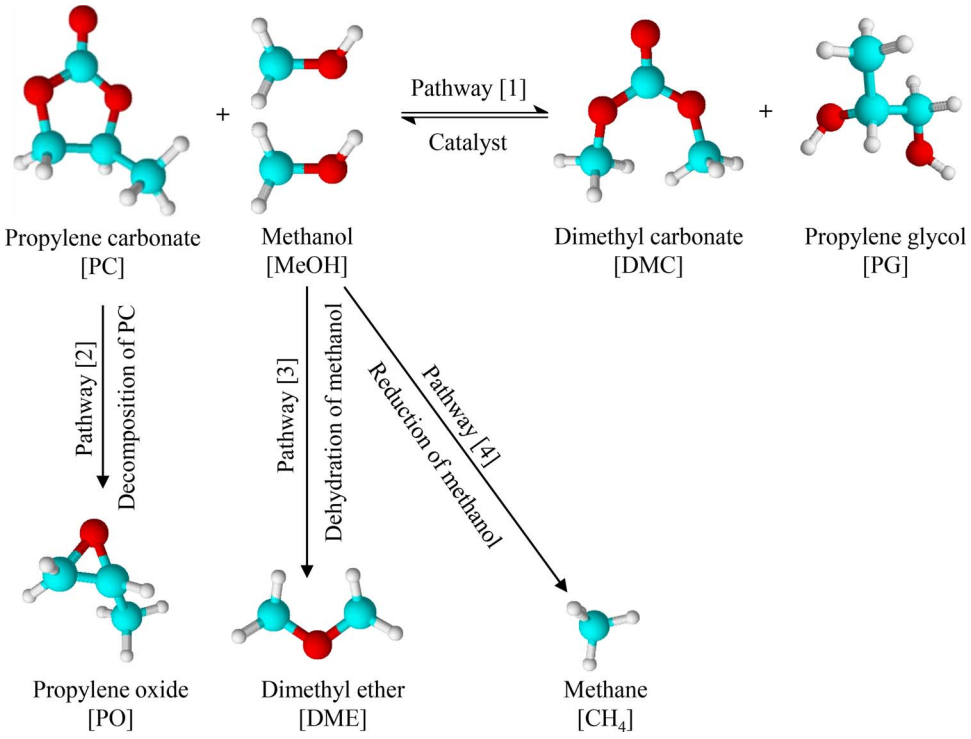

Fig. 7. Reaction scheme for the synthesis of DMC from PC and MeOH.

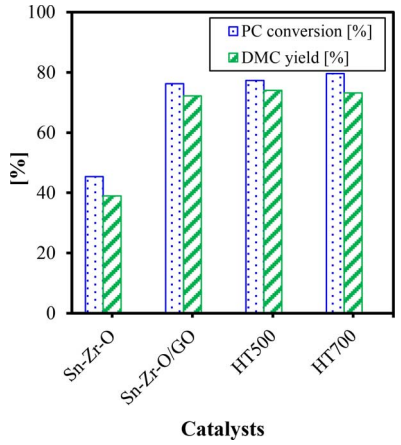

Fig. 8. Effect of different heterogeneous catalysts on the direct synthesis of DMC. Experimental conditions: MeOH:PC molar ratio 1:1; catalyst loading 2.5% (w/w); reaction temperature 433 K; reaction time 4 h and stirring speed 300 rpm.

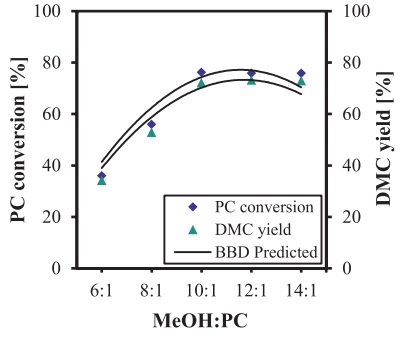

Fig. 9. Effect of MeOH:PC molar ratio on the synthesis of DMC. Experimental conditions: Catalyst: Zr–Sn/GO; catalyst loading 2.5% (w/w); reaction temperature 433 K; reaction time 4 h and stirring speed 300 rpm.

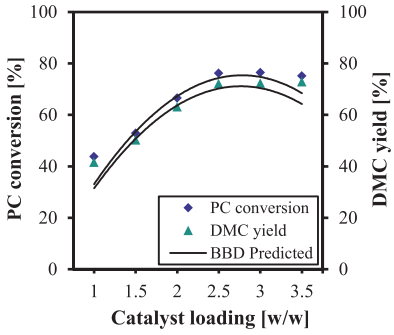

Fig. 10. Effect of catalyst loading on PC conversion and yield of DMC. Experimental conditions: Catalyst: Zr–Sn/GO; MeOH:PC molar ratio 10:1; reaction temperature 433 K; reaction time 4 h and stirring speed 300 rpm.

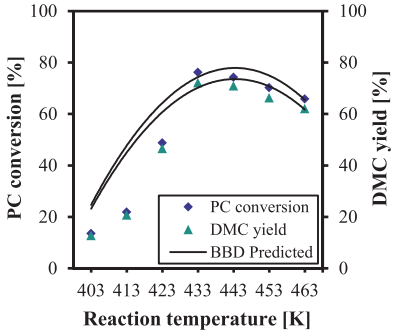

Fig. 11. Effect of reaction temperature on PC conversion and yield of DMC. Experimental conditions: Catalyst: Zr–Sn/GO; MeOH:PC molar ratio 10:1; catalyst loading 2.5% (w/w); reaction time 4 h and stirring speed 300 rpm.

results at various stirring speeds. As external mass transfer resistance is absent, it could be concluded that a good homogenous distribution of Zr–Sn/GO nanocomposite particles was achieved at a low stirring speed of 300 rpm.

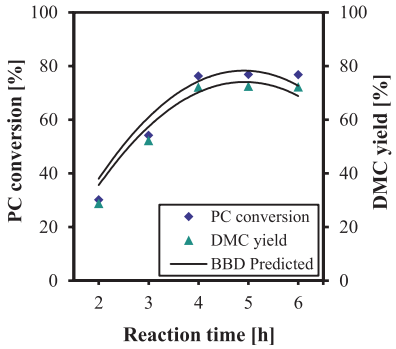

Fig. 12. Effect of reaction time on PC conversion and yield of DMC. Experimental conditions: Catalyst: Zr–Sn/GO; MeOH:PC molar ratio 10:1; catalyst loading 2.5% (w/w); reaction temperature 433 K and stirring speed 300 rpm.

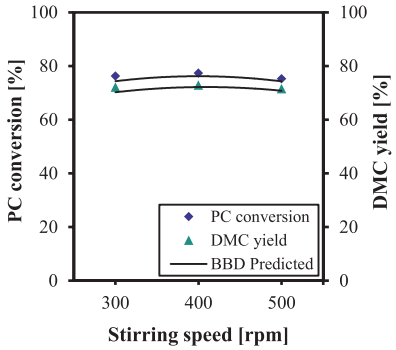

Fig. 13. Effect of stirring speed on PC conversion and yield of DMC. Experimental conditions: Catalyst: Zr–Sn/GO; MeOH:PC molar ratio 10:1; catalyst loading 2.5% (w/w); reaction temperature 433 K and reaction time 4 h. 2.

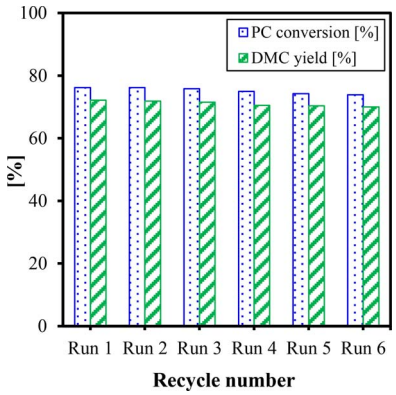

Fig. 14. Effect of catalyst reusability on PC conversion and yield of DMC. Experimental conditions: Catalyst: Zr–Sn/GO; MeOH:PC molar ratio 10:1; catalyst loading 2.5% (w/w); reaction temperature 433 K; reaction time 4 h and stirring speed 300 rpm.

3.5.7. Catalyst reusability studies

Catalyst reusability studies were carried out to investigate the long term stability of Zr–Sn/GO catalyst for the synthesis of DMC. The experiments were conducted in an autoclave reactor using a 2.5% (w/w) fresh catalyst, MeOH:PC 10:1 molar ratio at a reaction temperature of 433 K and reaction time of 4 h. This was plotted as Run 1 as shown in Fig. 14. After the first reaction, the catalyst was recovered by filtration from the reaction mixture, washed with acetone and dried in an oven at 333 K for 12 h. The catalyst was then reused for Run 2 under the same optimum reaction conditions (see Fig. 14). The same procedure was repeated for subsequent Runs (Run 3–Run 6). From Fig. 14, it can be seen that there is no appreciable change in PC conversion and yield of DMC after 6 Runs. This indicates that Zr–Sn/GO catalyst exhibits excellent reusability and stability for the synthesis of DMC. It is evident that Zr–Sn/GO nanocomposite catalyst can be easily recovered and reused without any significant loss in its catalytic performance.

3.6. Optimization of DMC synthesis

The aim of the optimization is to find the reaction conditions that can maximise PC conversion and yield of DMC even further. Batch studies using OFAT analysis showed that 10:1 MeOH:PC molar ratio, 433 K, 4 h and 300 rpm using 2.5% (w/w) Zr–Sn/GO achieves a PC conversion of 76.2% and DMC yield of 72.1%. Evaluating and including the interactions between the various reaction parameters can lead to higher PC conversion and DMC yield. Therefore, applying response surface methodology optimisation using BBD method can be used to understand the interactions between various reaction parameters and hence to derive maximum responses (i.e., PC conversion and DMC yield). The optimization process was developed using Design Expert 9.0.5 software. Consequently, the desired target was defined to maximise the yield of DMC and PC conversion with minimising the operational condition levels used in the regression model. The software combines the individual desirability into a single number, and then searches to optimise this function based on the response target. Accordingly, the optimum working conditions are determined.

The maximum predicted responses of 85.1% for PC conversion and 81% DMC yield were achieved at 12.33:1 MeOH: PC molar ratio, 2.9% (w/w) catalyst loading, 446.7 K, 4.08 h and 300 rpm using the BBD model. An additional experiment was then performed to confirm the optimised predicted results, where a PC conversion of 82.4% and DMC yield of 78.2% were obtained (within ± 3% experimental error). This demonstrates that the process optimization using BBD method was accurate.

RSM is also used to determine the interactions between independent variables and the responses which will show the effect of factors interaction on the desired response. Fig. 15 represents the 3-D graphical representation of the regression model. It shows the effect of MeOH:PC molar ratio and the catalyst loading at fixed reaction temperature, reaction time and stirring speed at their optimum conditions. It is clear that the yield of DMC increases with an increase in MeOH:PC molar ratio and catalyst loading. Maximum yield was observed at a reaction temperature of 446.7 K and catalyst loading of 2.9% (w/w), which indicates the accuracy of the optimization process that was established. The trend is reversed and the yield of DMC decreases to 20% as MeOH:PC molar ratio and catalyst loading increase beyond 12.3:1 and 2.9% (w/w), respectively.

Fig. 16 shows the effect of varying the stirring speed and reaction temperature at fixed MeOH:PC molar ratio, catalyst loading and reaction time at their optimum conditions. It can be seen that increasing the reaction temperature increases the yield of DMC, however, increasing the stirring speed shows no effect on the yield of DMC. This indicates the insignificance of stirring speed for the synthesis of DMC as predicted by ANOVA. The maximum DMC yield (81%) was observed at a reaction temperature of 446.7 K (Fig. 16). A decrease in the yield of DMC to 22% is obtained as the temperature increases beyond 446.7 K.

The interaction between reaction time and catalyst loading was studied at the optimum MeOH:PC molar ratio, reaction temperature and stirring speed as shown in Fig. 17. It is evident that an increase in the reaction time and catalyst loading increases the yield of DMC. DMC yield of 81% is observed at 4.08 h reaction time and 2.9% (w/w) catalyst loading, which agrees with the results obtained from optimization process and further verifies its accuracy. Fig. 17 also shows that long reaction time (i.e. higher than 4.08 h) and larger amounts of catalyst (i.e. more than 2.9% (w/w)) reduces the yield of DMC to as low as 9%.

4. Conclusions

The preparation of graphene nanocomposite catalyst *via* a continuous hydrothermal flow synthesis route allowed simultaneously and

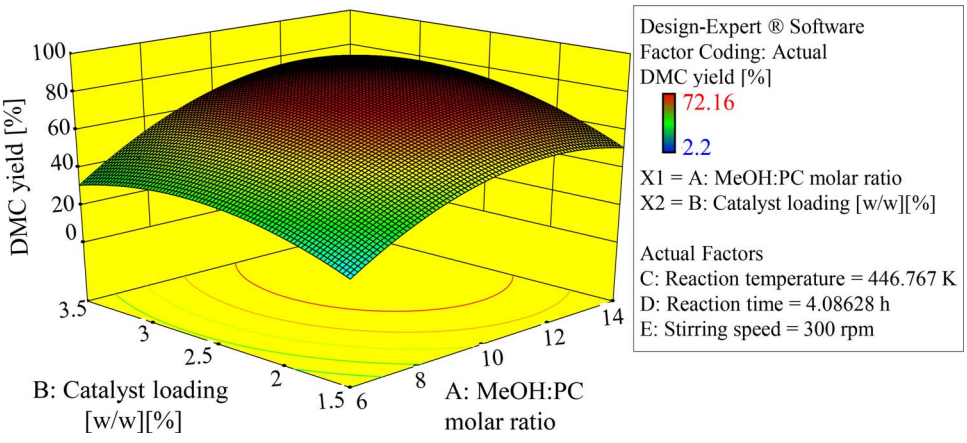

Fig. 15. Response surface graph: Effect of MeOH:PC molar ratio and catalyst loading (w/w) on DMC yield.

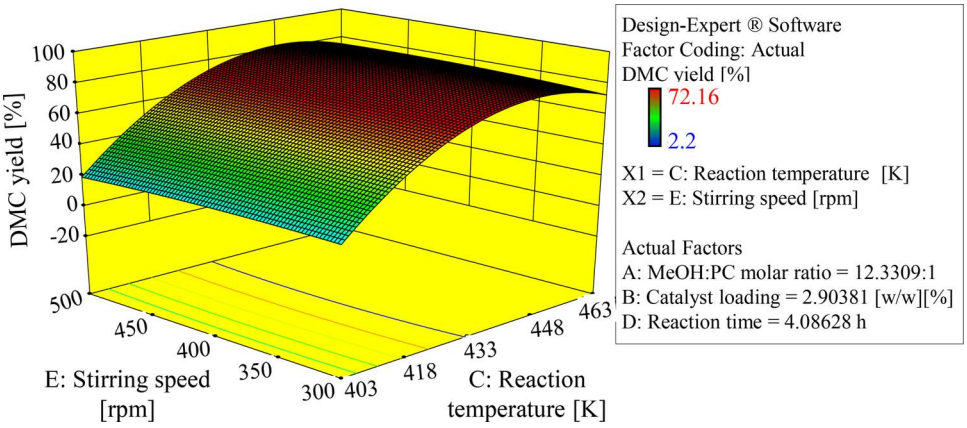

Fig. 16. Response surface graph: Effect of reaction temperature and stirring speed on DMC yield.

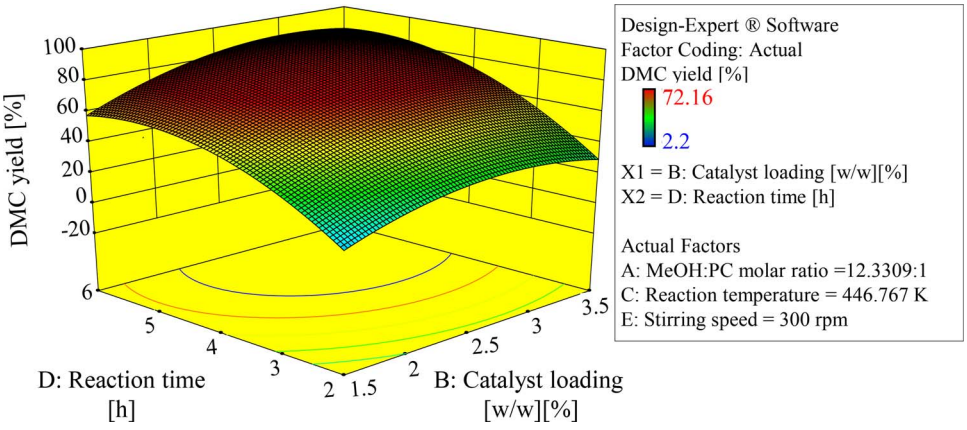

Fig. 17. Response surface graph: Effect of catalyst loading (w/w) and reaction time on DMC yield.

homogeneously growing and dispersing metal oxide nanoparticles into graphene substrate in a single step. This single step synthetic approach not only enables control over oxidation state of graphene, but also offers an optimal route for homogeneously producing and depositing highly crystalline nanostructures onto graphene. The synthesized Sn–Zr/GO nanocomposite catalyst was successfully utilised for the synthesis of DMC from PC and MeOH in the absence of a solvent. Tin doped zirconia/graphene nanocomposite catalyst showed the highest catalytic performance for DMC synthesis as compared to other heterogeneous catalysts.

RSM using BBD method was conducted to study and optimise the interactive effects of five process variables: MeOH:PC molar ratio, catalyst loading, reaction temperature, reaction time and stirring speed on the yield of DMC. A modified quadratic model equation was developed by analyzing the experimental data. The model predicted the highest PC conversion and DMC yield of ~85.1% and ~81%, respectively at an optimum reaction condition of 12.3:1 MeOH: PC molar ratio, 446.7 K, 4.08 h and 300 rpm using 2.9% (w/w) Zr–Sn/GO. Experimental results at optimum predicted reaction conditions verified the model predicted response where 82.4% PC conversion and 78.2% yield of DMC were obtained. Statistical analysis of the data showed that the MeOH:PC molar ratio, catalyst loading, reaction temperature and time are highly significant variables while stirring speed is an insignificant variable for the synthesis of DMC. Catalyst reusability studies indicated high stability of Zr–Sn/GO nanocomposite which could be reused multiple times without any significant reduction in its catalytic performance.

Acknowledgments

Rim Saada, Omar Aboelazayem and Suela Kellici gratefully acknowledge the financial support provided by London South Bank University. Omar Aboelazayem is also thankful to the British University in Egypt for supporting his research.

References

[1] Z.F. Zhang, Z.W. Liu, J. Lu, Z.T. Liu, Ind. Eng. Chem. Res. 50 (2011) 1981–1988.
[2] J. Bian, M. Xiao, S. Wang, Y. Lu, Y. Meng, Catal. Commun. 10 (2009) 1142–1145.
[3] J. Bian, M. Xiao, S.J. Wang, Y.X. Lu, Y.Z. Meng, Chin. Chem. Lett. 20 (2009) 352–355.
[4] D. Ballivet-Tkatchenko, S. Chambrey, R. Keiski, R. Ligabue, L. Plasseraud, P. Richard, H. Turunen, Catal. Today 115 (2006) 80–87.
[5] J. Bian, M. Xiao, S.J. Wang, Y.X. Lu, Y.Z. Meng, J. Colloid Interface Sci. 334 (2009) 50–57.
[6] M.S. Han, B.G. Lee, B.S. Ann, K.Y. Park, S.I. Hong, React. Kinet. Catal. Lett. 73 (2001) 33–38.
[7] H. Wang, M. Wang, S. Liu, N. Zhao, W. Wei, Y. Sun, J. Mol. Catal. A: Chem. 258 (2006) 308–312.
[8] R. Srivastava, D. Srinivas, P. Ratnasamy, J. Catal. 241 (2006) 34–44.
[9] S.M. Dhuri, V.V. Mahajani, J. Chem. Technol. Biotechnol. 81 (2006) 62–69.
[10] Y. Watanabe, T. Tatsumi, Microporous Mesoporous Mat. 22 (1998) 399–407.
[11] P. Unnikrishnan, D. Srinivas, Ind. Eng. Chem. Res. 51 (2012) 6356–6363.
[12] B.M. Bhanage, S.I. Fujita, Y. He, Y. Ikushima, M. Shirai, K. Torii, M. Arai, Catal. Lett. 83 (2002) 137–141.
[13] J. Xu, K.Z. Long, T. Chen, B. Xue, Y.X. Li, Y. Cao, Catal. Sci. Technol. 3 (2013) 3192–3199.
[14] J. Xu, K.Z. Long, F. Wu, B. Xue, Y.X. Li, Y. Cao, Appl. Catal. A: General 484 (2014) 1–7.
[15] M. Sankar, C.M. Nair, K.V.G.K. Murty, P. Manikandan, Appl. Catal. A: General 312 (2006) 108–114.
[16] D.W. Kim, D.O. Lim, D.H. Cho, J.C. Koh, D.W. Park, Catal. Today 164 (2011) 556–560.
[17] R. Juírez, A. Corma, H. Garcia, Green Chem. 11 (2009) 949–952.
[18] Y. Xie, Z. Zhang, T. Jiang, J. He, B. Han, T. Wu, K. Ding, Angew. Chem. Int. Ed. 46 (2007) 7255–7258.
[19] X.Y. Wang, S.Q. Liu, K.L. Huang, Q.J. Feng, D.L. Ye, B. Liu, J.L. Liu, G.H. Jin, Chin. Chem. Lett. 21 (2010) 987–990.
[20] A.I. Adeleye, S. Kellici, T. Heil, D. Morgan, M. Vickers, B. Saha, Catal. Today 256 (2015) 347–357.
[21] R. Saada, S. Kellici, T. Heil, D. Morgan, B. Saha, Appl. Catal. B: Environ. 168–169 (2015) 353–362.
[22] W.L. Dai, S.L. Luo, S.F. Yin, C.T. Au, Appl. Catal. A: General 366 (2009) 2–12.
[23] A.K. Geim, K.S. Novoselov, Nature Mater. 6 (2007) 183–191.
[24] A.K. Geim, Science 324 (2009) 1530–1534.
[25] S. Navalon, A. Dhakshinamoorthy, M. Alvaro, H. Garcia, Chem. Rev. 114 (2014) 6179–6212.
[26] D. Li, R.B. Kaner, Science 320 (2008) 1170–1171.
[27] Y.W. Zhu, S. Murali, W.W. Cai, X.S. Li, J.W. Suk, J.R. Potts, R.S. Ruoff, Adv. Mater. 22 (2010).
[28] C.N.R. Rao, A.K. Sood, K.S. Subrahmanyam, A. Govindaraj, Angew. Chem. Int. Ed. 48 (2009) 7752–7777.
[29] K.S. Novoselov, V.I. Fal'Ko, L. Colombo, P.R. Gellert, M.G. Schwab, K. Kim, Nature 490 (2012) 192–200.
[30] S. Bai, X. Shen, RSC Adv. 2 (2012) 64–98.
[31] Y. Wang, Z. Shi, Y. Huang, Y. Ma, C. Wang, M. Chen, Y. Chen, J. Phys. Chem. C 113 (2009) 13103–13107.
[32] Q. Xiang, J. Yu, M. Jaroniec, Chem. Soc. Rev. 41 (2012) 782–796.
[33] C. Liu, Z. Yu, D. Neff, A. Zhamu, B.Z. Jang, Nano Lett. 10 (2010) 4863–4868.
[34] E.V. Castro, K.S. Novoselov, S.V. Morozov, N.M.R. Peres, J.M.B.L. Dos Santos, J. Nilsson, F. Guinea, A.K. Geim, A.H.C. Neto, Rev. Phys. Rev. Lett. 99 (2007).
[35] J.H. Chen, C. Jang, S. Xiao, M. Ishigami, M.S. Fuhrer, Nature Nanotechnol. 3 (2008) 206–209.
[36] S.N. Baker, G.A. Baker, Angew. Chem. Int. Ed. 49 (2010) 6726–6744.
[37] S. Kellici, J. Acord, J. Ball, H.S. Reehal, D. Morgan, B. Saha, RSC Adv. 4 (2014) 14858–14861.
[38] V. Singh, D. Joung, L. Zhai, S. Das, S.I. Khondaker, S. Seal, Prog. Mater. Sci. 56 (2011) 1178–1271.
[39] V. Georgakilas, M. Otyepka, A.B. Bourlinos, V. Chandra, N. Kim, K.C. Kemp, P. Hobza, R. Zboril, K.S. Kim, Chem. Rev. 112 (2012) 6156–6214.
[40] S. Kellici, K. Gong, T.A. Lin, S. Brown, R.J.H. Clark, M. Vickers, J.K. Cockcroft, V. Middelkoop, P. Barnes, J.M. Perkins, C.J. Tighe, J.A. Darr, Philos.Trans. A: Math. Phys. Eng. Sci 368 (2010) 433–4349.
[41] A.A. Chaudhry, S. Haque, S. Kellici, P. Boldrin, I. Rehman, F.A. Khalid, J.A. Darr, Chem. Commun. (2006) 2286–2288.
[42] J.B.M. Goodall, S. Kellici, D. Illsley, R. Lines, J.C. Knowles, J.A. Darr, RSC Adv. 4 (2014) 31799–31809.
[43] Y. Hakuta, T. Adschiri, T. Suzuki, T. Chida, K. Seino, K. Arai, J. Am. Ceram. Soc. 81 (1998) 2461–2464.
[44] Z. Zhang, S. Brown, J.B.M. Goodall, X. Weng, K. Thompson, K. Gong, S. Kellici, R.J.H. Clark, J.R.G. Evans, J.A. Darr, J. Alloys Comp. 476 (2009) 451–456.
[45] T. Lin, S. Kellici, K. Gong, K. Thompson, J.R.G. Evans, X. Wang, J.A. Darr, J. Comb. Chem. 12 (2010) 383–392.
[46] V. Middelkoop, C.J. Tighe, S. Kellici, R.I. Gruar, J.M. Perkins, S.D.M. Jacques, P. Barnes, J.A. Darr, J. Supercrit. Fluids 87 (2014) 118–128.
[47] J.A. Darr, M. Poliakoff, Chem. Rev. 99 (1999) 495–541.
[48] K. Zhong, W. Lin, Q. Wang, S. Zhou, Int. J. Biol. Macromol. 51 (2012) 612–617.
[49] N.S. El-Gendy, S.F. Deriase, D.I. Osman, Energ. Sources Part A 36 (2014) 457–470.
[50] S. Tahmouzi, Carbohydr. Polym. 106 (2014) 238–246.
[51] X. Duan, Z. Zhang, C. Srinivasakannan, F. Wang, J. Liang, Chem. Eng. Res. Design 92 (2014) 1249–1256.
[52] M. Khajeh, E. Sanchooli, Food Anal. Meth. 3 (2010) 75–79.
[53] R. Bo, X. Ma, Y. Feng, Q. Zhu, Y. Huang, Z. Liu, C. Liu, Z. Gao, Y. Hu, D. Wang, Carbohyd.Polym 117 (2014) 215–222.
[54] L.S. Badwaik, K. Prasad, S.C. Deka, J. Int. Food Res 19 (2012) 341–346.
[55] D. Das, R. Vimala, N. Das, Ecol. Eng. 64 (2014) 136–141.
[56] C. Murugan, S.K. Sharma, R.V. Jasra, H.C. Bajaj, Ind. J. Chem. Sect. A 49 (2010) 288–294.
[57] D.B.G. Williams, M.S. Sibiya, P.S. van Heerden, M. Kirk, R. Harris, J. Mol. Catal. A: Chem. 304 (2009) 147–152.
[58] A. Pyrlik, W.F. Hoelderich, K. Miller, W. Arlt, J. Strautmann, D. Kruse, Appl. Catal. B: Environ. 125 (2012) 486–491.
[59] Y. Zhang, S.N. Riduan, Angew. Chem. Int. Ed. 50 (2011) 6210–6212.
[60] T. Wei, M. Wang, W. Wei, Y. Sun, B. Zhong, Fuel Process. Technol. 83 (2003) 175–182.